Chapter-2

Synthesis, Characterizations and Analysis Techniques

Chapter 2: Synthesis, Characterizations and Analysis Techniques

2.1 Overview

To achieve the goals outlined in chapter 1, it is necessary to synthesis the proposed systems and characterize them in terms of their subsequent structure, physical properties, and applications. The methods of synthesis, characterization with various techniques, and the methodologies used to determine the various parameters of the researched systems are all covered in this chapter. In the present work, the proposed compositions

(a) To synthesize $La_{9.67}Si_6O_{26.5}$,

(b) $La_{9.67-x}Sr_xSi_6O_{26.5}$ $(x = 0.05, 0.10\ and\ 0.15)$,

(c) $La_{9.67-x}Ca_xSi_6O_{26.5}$ $(x = 0.05, 0.10\ and\ 0.15)$,

(d) $La_{9.67-x}Ba_xSi_6O_{26.5}$ $(x = 0.05, 0.10\ and\ 0.15)$

by Solid state route. The solid-state reaction (SSR) method was used in the synthesis of the compounds. All the synthesized materials, each with its own unique composition, were put through a series of characterization to determine their structural, optical, thermal, and electrical capabilities. This chapter has been divided into three sections:

(1) Materials synthesis: This part covers the topics of sample preparation and the processing of a variety of different materials, each of which have their own unique composition.

(2) Characterization techniques: This section provides a concise overview of the structural, microstructural, thermal, optical, and electrical characterization methods that were performed during this work.

(3) Data analysis techniques: We've covered analysis techniques including Rietveld refinement of the XRD (X-ray diffraction) pattern, electrical conductivity, and impedance spectroscopy in this section.

2.1.1 Specification of Raw Materials

High purity raw materials were used to synthesize the investigated compositions. The specifications of raw materials are listed in Table 2.1.

Table 2.1: Description of the raw materials with their chemical formula, purity, and manufacturer used for the preparation of proposed compositions

S. No	Raw Materials	Chemical Formula	Purity	Manufacturer
1.	Lanthanum oxide	La_2O_3	99.9%	Alfa aesar
2.	Silicon Oxide	SiO_2	99%	Alfa aesar
3.	Barium carbonate	$BaCO_3$	99%	Merck
4.	Calcium Carbonate	CaCO3	99.5%	Alfa Aesar
5.	Strontium Carbonate	$SrCO_3$	99%	CDH

In order to synthesize the samples, several other high-grade chemicals, reagents, and solvents were utilized. Some examples of these include ethanol, acetone, ethylene glycol, isopropanol, nitric acid, deionized water, and hydrochloric acid, amongst others.

2.2 Materials Synthesis

Lanthanum Silicate ($La_{9.67}Si_6O_{26.5}$) and series can be synthesized by various methods. The preparative method has been adopted depending on the existing experimental facilities available in the research lab of department. A simple approach termed solid state ceramic technique was used to create pure, monovalent, and rare earth doped silicate in this study. It is a famous mechanical alloying method which used to synthesize various types of ceramic oxides. can be synthesized by several ways, such as hydrothermal, molten salt, sol-gel, citrate method, topochemical microcrystal, etc. Each method has its own advantage and disadvantage. In this work, we have synthesized the samples via solid-state reaction route. It's a well-known mechanical alloying procedure for creating several sorts of ceramic oxides.

After the samples have been synthesized, they must be described in order to determine their qualities and applications. Understanding the physics involved in each step starts with the characterization section. The characterization of pure and doped samples is carried out using a standard technique and modern, sophisticated tools in this thesis study. XRD (X-ray diffractometer) and SEM (scanning electron microscope) are used to investigate the structural and microstructural characterizations of the investigated samples (SEM). An EDX (energy-dispersive X-ray spectrometer) linked to a SEM (scanning electron microscope) and XPS (X-ray photoelectron spectroscopy) are used to analyze the samples' composition (XPS). Using a high-precision LCR meter, the electrical properties of the studied compositions are evaluated. The optical properties are studied using photoluminescence spectroscopy (PL) and UV-Vis spectrometer (UV-Vis). The optical band gap is calculated using well-established Tauc's relation. Thermogravimetric analysis (TGA) and DSC (differential scanning calorimetry) analyses were used to investigate the samples'

thermal properties. The electrical properties of prepared compositions are studied using a high precision LCR meter.

This chapter summarizes and presents the details of the preparative procedures, experimental techniques, and basic operating principles of the instruments employed.

2.2.1 SSR (Solid-State Reaction Route)

The SSR (solid-state reaction method) is a generally employed method for the synthesis of polycrystalline solids from solid constituent starting materials. It entails the mechanical blending of oxide and carbonate particles, followed by heat treatment. Typically, solids do not undergo reactions at room temperature during a typical timescale. Thus, it is required to heat them at a much higher temperature. The solid-state reaction rate is influenced by structural features of solids, reaction circumstances, surface area, temperature, pressure, and the change in thermodynamic free energy associated with the reaction. The advantages of using SSR method are listed below:

- Limited formation of side products
- No solvents are needed in the reaction.
- Structure purity along with desired properties.
- Large scale production
- Environment-friendly
- Simplicity and low cost

A detailed procedure of the solid-state reaction route is shown in the schematic diagram of Fig. 2.1.

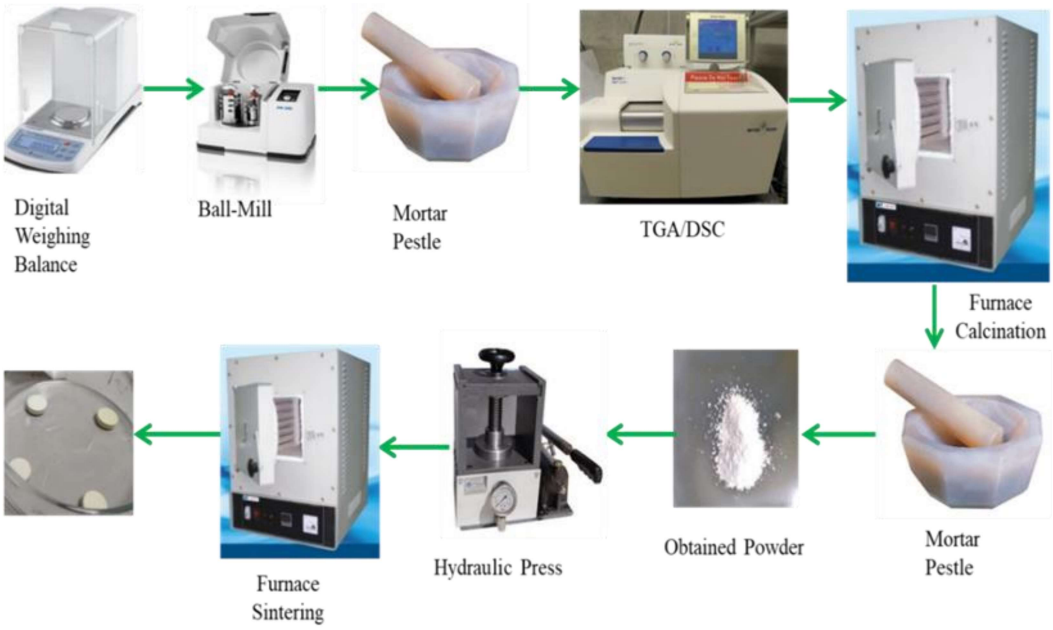

Fig. 2.1: Schematic of Solid-state reaction route.

2.2.2 Mechanism of Ball-Mill

Figure 2.1 presents an illustration of the process that underpins a planetary ball mill. The grinding action was entirely dependent on the rate and intensity of the collision of the balls with the sample. This rate and intensity were determined by the rotation speed of the disc (Ω), the speed at which the vials rotated around the disc (ω), the radius of the disc (R) and the vials (r), the mass or weight of the ball (m), and the number of balls (n). The shock power and the power supplied to the powder in each contact by the ball play a little role in the creation of end products in a planetary ball mill. The mathematical formula determines the power (P).

$$P \propto ml^2\Omega^2 \quad (2.1)$$

Where, l^2 is the characteristic area. The shock energy created between impacts of the balls with the inner wall of the closed vial is used to convert the precursor of raw materials into fine powder in a series of processes. During the beginning stages of the mixing process, the powder is first mixed, then fractured, then fused, and lastly the phase transformation and amorphization occur. Milling factors, such as milling environment, beginning powder composition, balls to powder mass ratio, materials of balls and vial, average milling time, and temperature created by the milling process all have a role in determining the nature of the final product.

Advantages

- Low-cost installation and grinding medium.
- One pot, one step mechano-synthesis.
- Fabrication of materials at room temperature.
- Revolution per minute (rpm) and milling time can be programmed for user defined.
- Suitability of choosing milling atmosphere.
- Applicable to materials having all degree of hardness.
- Synthesis of a new phase is possible with localized deformation.
- Formation of particles in the nano dimension or even in the amorphous phase and controls the particle size of final product.
- Formation of a complete solid solution.
- Complex powder formation in a concise time.
- Various milling parameters can control shock energy.

Disadvantages

- Contamination from the milling medium.
- Stickiness of the sample with container results loss of materials.
- Excessive heating during milling.

The optimization of milling parameters eliminates the disadvantages noted previously. To avoid contamination from the milling media, the milling period must be modified from time to time and sample to sample. The excess heat generated from the milling can be controlled by controlling the rpm of the vials. The balls to powder mass ratio (BPMR) and the milling atmosphere are chosen to ensure the purity of the final product.

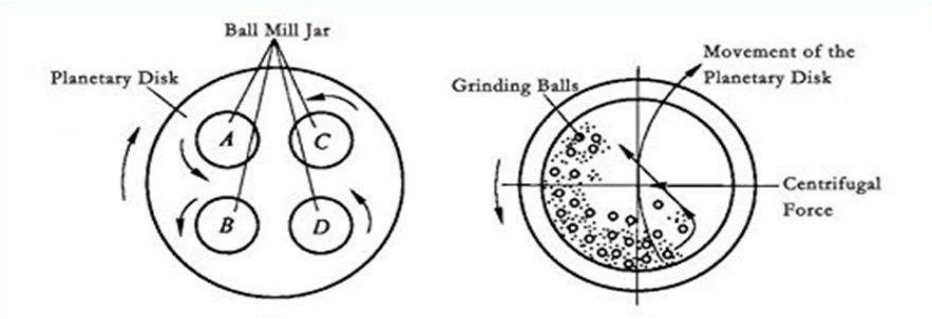

Figure 2.2: Working Principle of Lab Ball-Miller

2.2.3 Preparation of Materials using Ball Milling

In this thesis work, a vial is made up of chrome steel (The inside layer is coated with Zirconia) was simultaneously rotated with 5 zirconia balls each of 10 mm diameter kept inside the tightly closed steel vial. A stoichiometric amount of raw materials as shown in Table 2.1 are taken in a 100 ml chrome steel vial, partially filled with zirconia balls in the

ratio of 1:24 balls to mass ratio. The closed steel vial is then mounted on a planetary ball mill (PM 200, Retsch, Germany) and rotated with the speed of 50 rpm for 8 h with intermediate pauses. The high speed creates an impact between the balls and sample which is generated by the centrifugal force between the balls and inner-wall of the vial. The samples are stored with balls within the vial to facilitate uniform grinding. The powder is then transferred from the vial to an alumina crucible and dried in an oven for 24 hours at 60 degrees Celsius. The powders were then transferred to an agate mortar and crushed again to ensure uniformity.

2.2.4 Calcination of Materials

Calcination is the process of heating a solid to a high temperature that is below its melting point in order to induce a phase change or thermal disintegration that is different from melting or fusing. Thermal analysis (TGA/DSC) of the produced combination was done to find out the calcination temperature of the resulting powder. Furthermore, the produced mixture was transported to an alumina crucible and placed inside the programmable muffle furnace, where it was heated to 1200 °C for 12 hours to produce single phase powder. Following successful preparation, the intended compositions were submitted to a variety of different characterization approaches, which will be explained in the following section.

2.2.5 Granulation and pelletization

After calcination, the powder was uniformly mixed in an agate mortar with a pestle. The powder was then uniformly blended with 1 percent polyvinyl alcohol (PVA) until it became fine. The fine powder was then pelletized using a hydraulic press and a die with a diameter of 12 mm while applying a pressure of 7 tons. After that, the pellets are used for further characterization.

2.3 Pelletization for Conductivity and Dilatometry Measurements

Pellets of the synthesized samples were formed using a hydraulic press machine (shown in Fig. 2.3). It involves mechanical or hydraulic pressure to pack the powder into a pellet in the die set. The pressure needed to form a pellet of adequate mechanical strength depends on the properties of the materials used, including but limited to particle size, adhesive material, and moisture level. Besides, binding agents like stearic acid, polyvinyl alcohol, and ethanol also assist pellet formation. Once the pellet is formed, pellets are placed into a furnace and heated at the desired temperature. This removes the binder residue and increases the density and mechanical strength of the material.

Within this thesis, all the pellets were formed using a manual hydraulic press, die of 12 mm diameter and pressure of 7 tons.

Figure 2.3: Experimental setup of hydraulic press machine

2.3.1 Sintering

Sintering is the process of heating for microstructural change, densification and crystal growth of the material. Sintering of the materials has carried out in several steps of thermal heating. The furnace was heated to 1375 ºC at a rate of 5 ºC per minute, then left at that temperature for 14 hours to begin the sintering process. The pellets were then cooled at rate of 5 ºC /min to room temperature. The further characterization techniques to study the phase formation, microstructure and electrical properties of pellets were carried out and described in subsequent section.

2.4 Characterization Techniques

2.4.1 TGA-DSC (Thermal Analysis)

The thermo-gravimetric analysis (TGA) is a technique for determining the sample's calcination temperature as well as evaluating the material's stability. This analysis, which provides details on the mass gain (absorption), mass loss (desorption), phase transition, and other features of the sample, has measured the change in mass of the experimental sample as a function of temperature[57]. when a sample's mass stays constant across a temperature range, the sample is thermally stable within that range. TGA also reveals the sample's top temperature limit, beyond which the material begins to degrade. TGA is commonly used in the literature to determine the reaction temperature of a sample, material stability, and so on[58].

After a sample has been subjected to a controlled temperature program, DSC (Differential Scanning Calorimetry) assesses the change in the difference in heat-flow rate between the sample and the reference sample. The alteration of heat capacity is documented

in terms of variations in heat flow while a sample of known mass is heated or cooled. The kind of reaction (Endothermic or Exothermic), enthalpy, Gibbs energy, and other thermal characteristics can all be calculated using this method. The combined TGA-DSC analysis also provides insight into the reaction route for the manufactured raw material mixture as well as numerous transition points such as melting point, glass transition temperature, crystallization temperature, and so on. The TGA-DSC measurement in this thesis was performed using a TGA/DSC (Mettler Toledo, Germany) model that was executed in the temperature range of (27 to 1000) °C in the presence of nitrogen gas.

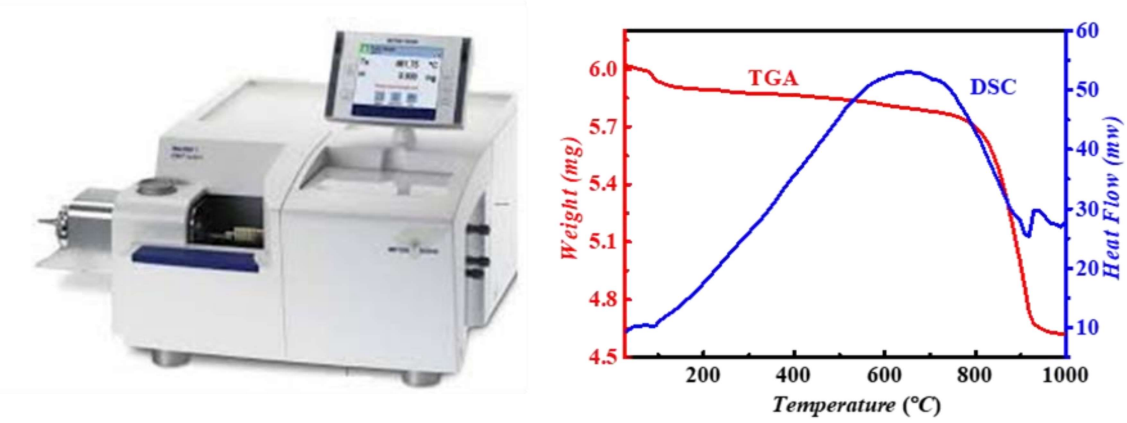

Figure 2.4: (a) TGA-DSC facility **(b)** experimental setup of TGA/DSC (right).

Tthermogravimetric Analysis (TGA) is a technique for measuring the change in mass of a sample as a function of temperature or time in a controlled environment. It's used to figure out the sample's calcination temperature and thermal stability. A sample is said to be thermally stable within a certain temperature range if its mass remains constant within that temperature range. TGA also tells you what temperature is the upper limit beyond which the sample starts to degrade. Weight losses are fundamental features of the sample and can be

utilized to calculate quantitative compositional changes, among other things. This technique can also be used to confirm a phase transition in a sample.

TGA measurements were taken in the nitrogen and oxygen atmospheres using the TGA/DSC 1 (Mettler Toledo, Germany) model, which was operated in the temperature range of 27 °C to 1000 °C. The schematic diagram and experimental set up of the TGA/DSC technique are shown in Fig. 2.4.

2.4.2 Measurement of Density and Porosity

The density (ρ) of prepared samples was calculated using the Archimedes principle. Pellets of each composition were created for this purpose. Each composition's powders were combined with 1% polyvinyl alcohol (PVA) and pelletized using a vertical die with a diameter of 10.0 mm and a thickness of 2.0 mm and a normalized load of 6 Ton by hydraulic press. In this process, pellets are initially weighed in air before being immersed in the immersion liquid. For this thesis, acetone($\rho_{ace} = 0.79 g cm^{-3}$ was used as the immersion solvent. If m_{dry} and m_{ace} are the weight of the pellet in air and acetone medium, then the sample's real density is given by

$$\rho = \frac{\rho_{ace} * m_{dry}}{m_{dry} \sim m_{ace}} \tag{2.2}$$

In this thesis work, two different pellets of each type were weighed three times, and the average of those three weights was used as the sample's experimental density. The weight was measured with a digital scale that was accurate to within ± 0.00001 gm. as shown in **Figure 2.5**.

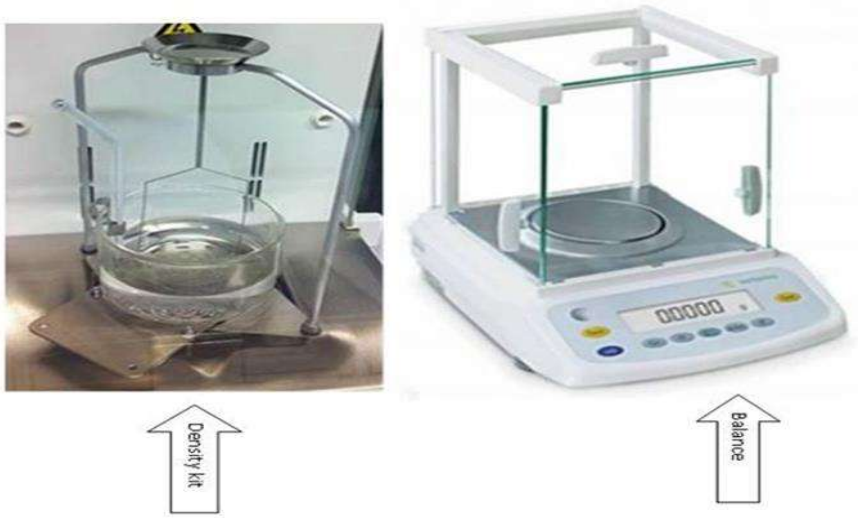

Figure 2.5 Density kit and weighing balance [Sartorius, BSA2245CW]

Using the link between the compound's molecular weight and the lattice characteristics, theoretical density was calculated,

$$D_{th} = \frac{n \times M}{N \times V} \tag{2.3}$$

Where, D_{th}=theoretical density, n= number of formula unit per unit cell, M= molecular weight of the sample, N=Avogadro's Number and V= unit cell volume. % porosity can be calculated by using the following relation

$$\%\ porosity = \left(\frac{D_{th} - D_{exp}}{D_{th}}\right) \times 100 \tag{2.4}$$

2.4.3 X-Ray Diffraction Analysis (XRD)

The powder X-ray diffraction technique (XRD), a non-destructive and flexible analytical method used to reveal extensive information on the crystallographic structure of the materials, will be covered in this article. The XRD technique relies on elastic scattering,

which refers to the modification of the propagation direction of electromagnetic waves. The diffraction pattern is the consequence of the coherent addition of all the electromagnetic waves that are diffused from atoms that belong to the same family of planes. This results in the pattern. Each of the materials generates a unique XRD pattern, which is indexed for the purpose of identifying the different phases that are present in the substance. When it comes to phase identification using XRD, the most significant considerations are the peak position and the relative strengths of these peaks in the diffraction profile. Most commonly, the X-ray radiations are emitted by copper specimen, and its characteristic wavelength is 1.5418 Å for K_α radiation. Figure 2.6(a) and 2.6 (b) depicts the block diagram of powder X-ray diffractometer and Braggs scattering from the lattice plane.

2.4.3.1 Bragg's law

The XRD (X-ray diffraction) method follows Bragg's law of X-ray diffraction. This law can be explained geometrically, as depicted in Fig. 2.6. In XRD, a collimated beam of X-rays is incident on the crystallographic lattice plane with an interplanar spacing d_{hkl}. Let θ be the incident angle between the X-ray beam and lattice plane, the interplanar spacing d_{hkl} creates a path difference for the ray scattered from the top & bottom surface of the plane. Using the geometry, the path difference between incident and diffracted ray is found to be $2d_{hkl}\text{Sin}\theta$. If the path difference is an integral multiple of wavelength (λ), then we have the constructive interference pattern between the scattered rays. Mathematically, Bragg's law is given as:

$$2d_{hkl}\text{Sin}\theta = n\lambda \qquad (2.5)$$

where n = integer and it shows the order of diffraction.

The geometry used in the X-day diffractometer is depicted in Fig. 2.6(b). The angle of incidence and scattered ray with respect to specimen surface is θ. The XRD pattern is recorded by deviating the incident X-ray beam angle by θ and scattering angle by 2θ. The scattered intensity is recorded as the function of 2θ. In some of the cases, While the sample and detector rotated by angles θ and 2θ, respectively, the X-ray source was kept in place. However, in most cases, the sample retains a stationary position while both the detector and source simultaneously rotate by θ angle. The central part of the diffractometer is Goniometer, and such precise rotation is performed by it. Typically, the detector and X-ray source travel around the sample's periphery while it is positioned on a rotational axis. Normally, the 2θ range between 20° - 80° is sufficient to cover the most useful part of the diffraction pattern.

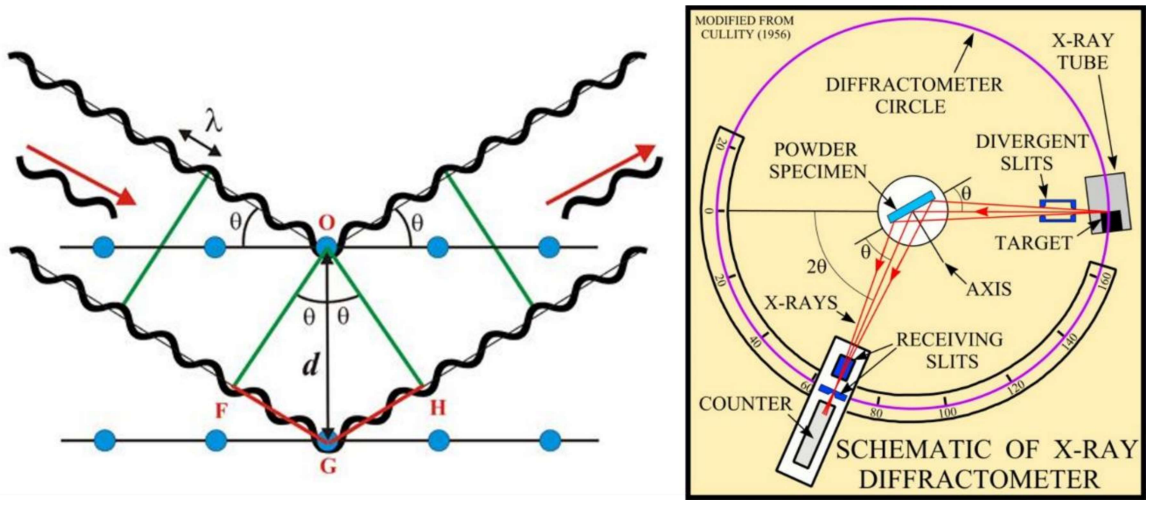

Figure 2.6: (a) Visualization of Bragg's law **(b)** Schematic representation of θ/2θ diffraction in Bragg-Brentano geometry.

To check the phase formation of the studied compositions, the XRD pattern was recorded using an X-ray diffractometer (Rigaku Miniflex II) applying Cu-Kα radiation with Ni filter and applied voltage of 40kV. The X-ray diffractometer used in our investigation is shown in Fig. 2.7. The XRD (X-ray diffractometer) peaks are generated from the randomly oriented planes identified by the respective Miller indices (hkl).

Figure 2.7: Experimental setup of X-ray diffractometer [Rigaku Miniflex II]

The X-ray peaks are matched and indexed by the standard phase which contains miller indices, diffraction angle or similar interplanar spacing, relative intensity and other crystallographic information. The standard database is prepared and maintained by "**International Center for Diffraction Data (ICDD)**" previously known as the "**Joint Committee for Powder Diffraction Standards (JCPDS)**". A simulation methodology, in which the theoretical XRD pattern is created by a computer program using structural information from the ICDD database, is an alternate way. Only when the crystal phase or equivalent structure file is accessible in the ICDD database can this method be used.

The calculated XRD pattern is then fine-tuned to fit the experimental XRD data using a continuous iteration procedure that adjusts instrumental, microstructural, and structural parameters.

In addition, the XRD pattern can also be used to calculate the crystallite size (d) of a material. Strain and the size of the crystalline domains both effect peak broadening. The Scherrer formula $\boldsymbol{d = \frac{0.9\,\lambda}{\beta \cos\theta}}$ can be used to calculate domain size, which was previously known as crystallite size. The FullProf suite was utilized to do the Rietveld refinement analysis of the XRD pattern, which is covered in more detail later in this chapter.

2.4.3.2 Phase Formation and Crystal Structure Studies by Powder X- ray Diffraction

Powder XRD (X-ray diffraction) has long been recognized as a versatile and important characterization tool for phase identification. The technique of connecting XRD patterns from a packed powder specimen is known as powder X-ray diffraction. The XRD pattern is formed by several microscopic polycrystals with randomly oriented domains in all possible directions in the powder samples. Coherently diffracting domains are those that produce diffraction in the same direction. The crystal structure, preferred orientation of lattice planes, crystallite size, shape, and size distribution of polycrystalline powder are all determined using this technique. The samples can be exposed to a range of pressure and temperature settings while the diffraction pattern is being collected because it is a non-destructive procedure.

The Rietveld refinement analysis of the powder XRD (X-ray diffraction) pattern from a polycrystalline sample has been performed on well resolvable diffraction data. For this

purpose, the XRD data were recorded in step scan mode with a slow scanning rate. The different crystallographic phases of the present sample were extracted by capturing X-ray diffraction pattern at ambient temperature using, XRD (X-ray diffractometer) (Rigaku Miniflex II, Japan) equipped with Cu Kα radiation having wavelength λ=1.5418 Å at an applied voltage of 40 kV and current 40 mA. The XRD pattern has been recorded in the angular range of 20 º -80 º with step size 0.02 º and scan @ 0.02 º/min. We have used the width of the primary divergence slit was 0.6 mm, and for the secondary detector, the slit was at 1.0 mm for X-ray diffraction measurements. The X-ray diffractometer used for present thesis work is shown in Fig. 2.8.

Figure 2.8 XRD facilities, Central Instrument Facility (CIF) IIT (BHU).

2.4.3.3 Phase Matching

In the powder XRD pattern, the peaks are generated from the randomly oriented planes identified by the respective Miller indices (hkl). The XRD peaks are indexed and matched by standard phase identification method which contained Miller indices, relative intensity with similar interplanar spacing or diffraction angles and other crystallographic

information[59]. In present thesis work, the experimental XRD pattern is matched with the COD database. Another alternative method besides this search match method is the simulation method in which the theoretical XRD pattern is generated by computer program through structural information available from the ICDD database. This method is only applicable when the crystal phase(s) or similar structure file is available in the ICDD database. The gross computed XRD pattern is then refined to fit the experimental XRD pattern by modifying several instrumental, structural and microstructural parameters through the continuous iteration process[60].

2.4.3.4 Rietveld Refinement Study

International Union of Crystallography (IUCr) proposes the Rietveld method as "Method of analyzing powder diffraction data in which the crystal structure is determined by fitting the complete profile of the diffraction pattern to a computed profile using a least-squares approach." Analysis of patterns with several overlapping Bragg peaks is achievable since there is no intermediate step for obtaining structure factors [60]. The experimental XRD pattern is analyzed by identifying the crystalline phase(s) that correspond to the available materials in the COD database. After phase identification, the crystallographic information file (CIF) containing the individual detailed structure is taken for further processing. With the help of a CIF file, Rietveld refinement software simulates a theoretical XRD pattern. For structural and microstructural characterizations to be studied, the following information must be given: (a) instrument correction factors, such as peak shift, peak broadening, and asymmetry in peak; and (b) a rough estimate of crystallite size and lattice strain. To get the structural and microstructural parameters, the simulated XRD pattern is used to fine-tune the experimental XRD pattern while keeping another parameter the same.

In this case, the Marquardt least squares method was used to find the best fit. By making small changes to the structural and microstructural parameters one at a time until the parameters converge, you can get the best match between the intensities of the simulated XRD pattern and the experimental XRD pattern. The quantity S_y is minimized through least square method defined as-

$$S_y = \sum_i W_i(I_{oi} - I_{ci})^2 \quad (2.6)$$

Here, $W_i = 1/I_{oi}$, I_{oi} = observed intensity at i^{th} step and I_{ci} = calculated intensity at i^{th} step. The best fit is achieved when S_y attains a minimum value. The value of I_{ci} is obtained by summation of all calculated intensities and background contribution given by

$$I_{ci} = S\sum_k L_k|F_k|^2 \emptyset(2\theta_i - 2\theta_k)P_k A + I_{bi} \quad (2.7)$$

Here, S is the scale factor, L_k contains Lorentz polarization factor and multiplicative factor, k represents Miller indices hkl for a Bragg reflection, F_k is the structure for k^{th} Bragg reflection, $\emptyset$ is a reflection profile function which approximate the effect of aberration due to absorption, specimen displacement, crystallite size, microstrain etc., P_k is the preferred orientation function, A is an absorption factor, I_{bi} is the background intensity of i^{th} step, $2\theta_k$is the diffraction angle of k^{th} Bragg reflection.

The Rietveld refinement of the XRD (X-ray diffraction) pattern is a very important step because it involves a lot of parameters and needs a lot of calculations. For this, you need advanced software that can match up the calculated and experimental XRD patterns at each step. This software should also be easy to use. Some Rietveld software is free and is used by

many people around the world. In this thesis, the Rietveld refinement was done using the FullProf software package.

The X-ray powder diffraction data made by H.M. Rietveld in 1969. are used with the Rietveld refinement software. This software package is also used to match profiles without knowing anything about the structure of the crystal. This software can evaluate the different structural and microstructural parameters by considering all the latest developments. A typical interface of FullProf software is shown in Fig.2.9. This software is used to analyze X-ray diffraction of different samples from bulk to nano dimension.

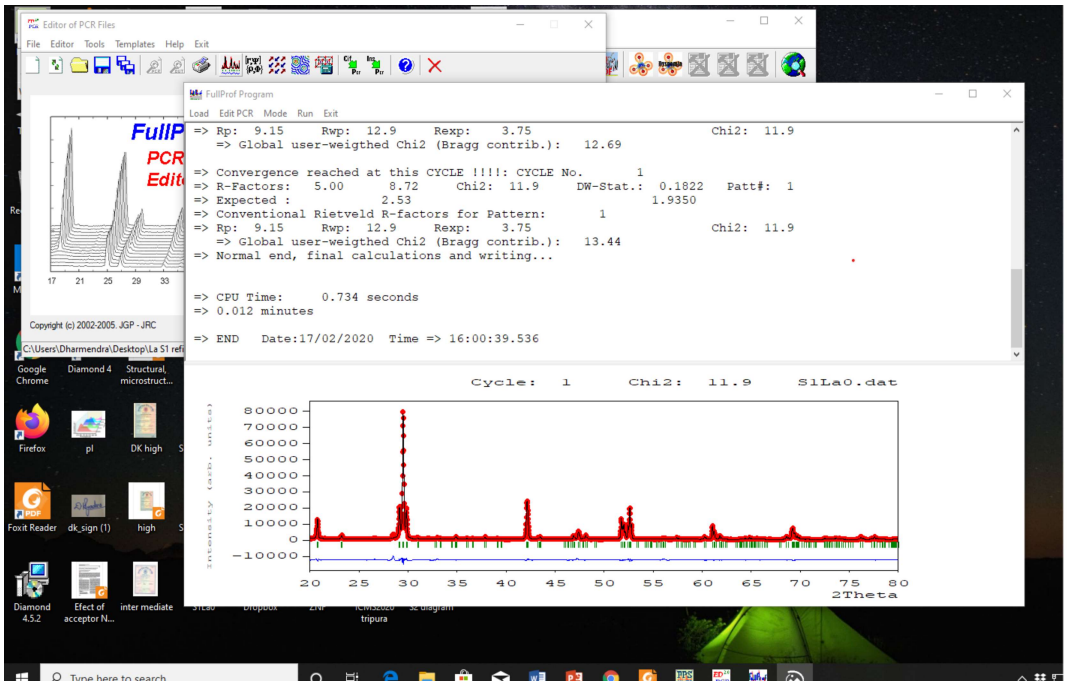

Figure 2.9 A typical FullProf software interface during Rietveld refinement process.

The main features and advantage of FullProf software are-

1. This software can be used to fine-tune the X-ray diffraction data that was collected with a lab set-up, synchrotron sources, and neutron diffraction sources.
2. Several functions, such as constant function and higher order polynomial by Fourier filtering, are used to define the backgrounds.
3. Gaussian, Lorentzian, modified Lorentzian, pseudo-Voigt, Pearson-VII, Thompson-Cox-Hashing (TCH) pseudo-Voigt, numerical, split pseudo-Voigt, and the convolution of a double exponential with a TCH pseudo-Voigt are all used to represent the peak form for each phase.
4. Multiple phases can be refined using the Rietveld method (up to 16 phases).
5. For the modeling of desired peak orientation, two types of functions are available.
6. There are absorption corrections for various geometries as well as micro-absorption corrections for Bragg-Brentano setup.
7. It allows you to generate hkl and/or symmetry operators automatically.
8. Magnetic structure refinement can also be performed.
9. Reflections are generated automatically for an incommensurate structure with up to 24 propagation vectors.
10. For certain types of defects, the position shifts of Bragg reflections are hkl dependent.
11. Without the requirement for structure factor computations, quantitative analysis was carried out.
12. The instrumental resolution function (Voigt function) can be stored in a file, and then the microstructural analysis can be carried out.
13. Popa-Balzer model can add anisotropic crystallite size and strain.

14. The square root of intensity is shown against 2θ for a better view of the simulated and experimental patterns.

The scale factor of Rietveld refinement determines the quantitative measure of different phases present in a multiphase compound. The weight fraction phase of a multiphase system with a known molecular weight can be estimated using the relation

$$W_i = \frac{S_i(ZMV)_i}{\sum_j S_j(ZMV)_j} \tag{2.8}$$

Here, S_i = scale factor, Z_i = the number of molecules per unit cell, M_i = the molecular weight and V_i = the unit cell volume of i^{th} phase present. The density of i^{th} phase can be evaluated using the following relation-

$$\rho_i = \frac{Z_i M_i}{N_A V_i} \tag{2.9}$$

N_A is Avogadro number. It is important to calculate the relative phase abundances in a multiphase compound for its different scientific and industrial applications. Rietveld analysis was found to be a very successful method to determine the phase fraction of multiphase material. X-ray diffraction profile fitting by Rietveld refinement method utilizes the minimization of different structural and microstructural parameters by an iterative method [61]. These methods refine and adjust different parameters until the residue between experimental intensities (I_{oi}) and calculated intensities (I_{ci}) is minimized. Following residue parameters are used to define the quality of fitting.

The residue of structure factor

$$R_F = \frac{\sum_i |\sqrt{I_{oi}} - \sqrt{I_{ci}}|}{\sum_i |\sqrt{I_{oi}}|} \quad (2.10)$$

The residue of Bragg factor

$$R_B = \frac{\sum_i |I_{oi} - I_{ci}|}{\sum_i |I_{oi}|} \quad (2.11)$$

The residue of weighted pattern

$$R_{wp} = \left| \frac{\sum_i W_i (I_{oi} - I_{ci})^2}{\sum_i W_i (I_{oi})^2} \right|^{\frac{1}{2}} \quad (2.12)$$

The residue of expected pattern

$$R_{exp} = \left| \frac{N - P}{\sum_i W_i (I_{oi})^2} \right| \quad (2.13)$$

In all the equation I_i is the intensity of i^{th} Bragg reflection at the end of the refinement, the letter o and i in suffix represents the observed and calculated intensities. W_i and N represents the weight and number of experimental observation and P represents the number of refineable parameters. The refinement process has been continued till convergence of this parameter is reached. The quality of fit is also monitored by "Goodness of fit" (GOF) defined as

$$GOF = \frac{R_{wp}}{R_{exp}} \quad (2.14)$$

For best fit, the GOF is approx. 1.00 which means the calculated pattern fully matched with the experimental pattern.

2.4.3.5 Size-Strain Analysis

The microstructural study of polycrystalline compounds has been investigated in terms of crystallite (particle) size, lattice strain, and flaws (dislocations and stacking faults) by analyzing the XRD pattern using the following techniques: **(a)** The integral width method (Williamson-Hall plot) **(b)** The Variance method **(c)** Fourier Transformation Method (Warren-Averbach line profile analysis). Practically, no polycrystalline sample is ideal so that the diffraction peaks are broadened with finite peak width. The broadening in XRD peaks is appeared due to **(a)** Instrumental broadening **(b)** Small crystallite size **(c)** Accumulation of lattice strain **(d)** Presence of different kinds of stacking faults in the lattice.

The analysis of diffraction pattern by integral breadth method can predict the finite particle size and microstructure of the composition. Scherer introduced this method in 1918 and Stokes and Wilson further modified it [62]. This is the oldest method widely used for determination of particle size and strain. In this method, the width of diffraction line is defined as the angular width of the peak in radians at a point where the intensity reduces to half of its highest value, i.e., full width at half maxima (FWHM). Max-Von Laue proposed another method to measure the breadth of diffraction peak as:

$$\beta = \frac{1}{I_p}\int I(2\theta)d(2\theta) \tag{2.15}$$

Here, β is integral width, I_p is the peak intensity and $I(2\theta)$ is intensity at diffraction angle 2θ. In 1949, Hall suggested the integral breadth should be described as the summation of two broadening given by (After correction of instrumental broadening and neglecting broadening due to lattice imperfections).

$$\beta = \beta_D + \beta_S \quad (2.16)$$

Here, β_D and β_S are peak broadening due to small crystallite size and microstrain in lattice respectively. The β_D is measured by Scherrer equation-

$$\beta_D = \frac{k\lambda}{DCos\theta} \quad (2.17)$$

Where λ is X-ray wavelength, k is the crystallite shape constant ($k = 0.89$ for spherical shape), D is the crystallite size and θ is the Bragg angle. β_S is the broadening arising from the microstrain in the compound given by

$$\beta_S = 4\epsilon\, tan\theta \quad (2.18)$$

Where ϵ is the microstrain in the lattice, so **Eq (2.15)** can be rewritten as

$$\beta = \beta_D + \beta_S = \frac{k\lambda}{DCos\theta} + 4\epsilon\, tan\theta \quad (2.19)$$

$$\frac{\beta Cos\theta}{\lambda} = \frac{1}{D} + \frac{4\epsilon Sin\theta}{\lambda} \quad (2.20)$$

Thus, by measuring the FWHM (β) and corresponding Bragg angle of all reflection appeared in the XRD pattern of the polycrystalline sample. A straight line (best fit) using Eq (2.19) obtained by plotting the curve between $\frac{\beta Cos\theta}{\lambda}$ along ordinate and $\frac{Sin\theta}{\lambda}$ along abscissa is known as Williamson-Hall Plot. The intercept of the straight line on ordinate gives the measure of $\frac{1}{D}$ and slope of the straight line gives the measure of average micro strain (ϵ).

In Williamson-Hall plot the line broadening in XRD peaks is primarily considered to be isotropic. This indicates that the diffracting domains were isotropic and micro strain contribution was also present. However, in the case of isotropic line broadening, a better evaluation of size-strain parameters was obtained by "Size-Strain plot (SSP)" method. The advantage of this method is that less weightage has been given to the data obtained at high angles, where the prerecession is usually lower. In this approximation, the crystallite size profile is considered to be a Lorentzian function and the strain profile by a Gaussian function. Accordingly, we have

$$\left(\frac{d_{hkl}\beta cos\theta}{\lambda}\right)^2 = \frac{k\lambda}{D}\left(\frac{{d_{hkl}}^2\beta cos\theta}{\lambda^2}\right) + \left(\frac{\varepsilon}{2}\right)^2 \quad (2.21)$$

Where d_{hkl} is the interplanar spacing corresponding to the plane (hkl), ε is the average strain produced in the lattice, k is a constant which depends on the shape of particles, for example, it is ¾ for a spherical particle. Like the W-H plot, the term $\left(\frac{d_{hkl}\beta cos\theta}{\lambda}\right)^2$ plotted with respect to $\left(\frac{{d_{hkl}}^2\beta cos\theta}{\lambda^2}\right)$ for all diffraction peaks. The particle size was determined from the slope of the linearly fitted data while the square root of the intercept gives the strain.

2.4.4 XPS (X-Ray Photoelectron Spectroscopy)

XPS is a non-destructive surface-sensitive spectroscopic technique that determines the elemental composition of a material down to the part per thousand level, as well as the chemical and electronic states of the elements present, as well as empirical equations. It not only reveals the elements present, but also the elements to which they are connected. XPS is a high-vacuum method that works at a pressure of ~ 10^{-6} Pa. The latest frontier is an ambient

pressure XPS system that can analyze samples at pressures as low as a few tens of millibars. This technique is based on the process of photoemission. In this technique, the material surface is bombarded with the high energy X-ray; consequently, the inner level electrons of the surface atom, within 1-10 nm, absorb the photon energy hυ, overcome their binding energy E_B, and emitted out of the surface with the kinetic energy E_{kin} (depicted in Fig. 2.10). This process is described by the following Einstein equation:

$$E_{kin} = h\upsilon - E_B - W_f \qquad (2.22)$$

where $h\upsilon$ = the energy of the incident X-ray source, E_{kin} = K.E.(kinetic energy) of emitted electrons, W_f = work function of the material, and E_B = binding energy of core electrons. MgKα and AlKα are the two source sources generally used because of their high energy and narrow width.

After analyzing the emitted photoelectrons' energy spectrum, a spectrum of intensity as a function of binding energy is produced. Each peak's binding energy reflects the element's properties. ESCA is another name for XPS (Electron Spectroscopy for Chemical Analysis). XPS is routinely used to investigate semiconductors, metal alloys, inorganic compounds, catalysts, glues, polymers, ceramics, glasses, inks, woods, bones, teeth, medical implants, elements, bio-materials, viscous oils, ion-modified materials and many others.

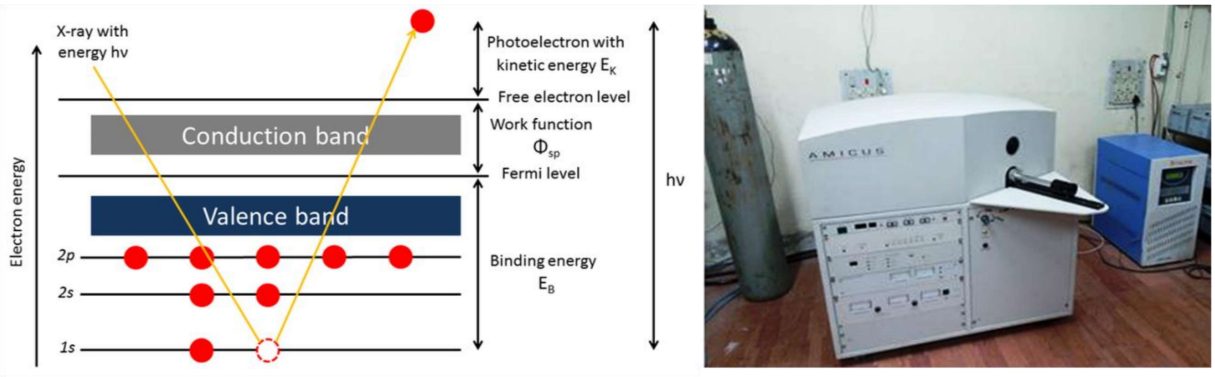

Figure 2.10: (a) Mechanism and **(b)** Experimental setup for the XPS spectroscopy (Kratos Amicus).

In the present thesis work, XPS spectra of the samples have been recorded using Kratos Amicus XPS setup utilizing Mg target under 10^{-6} Pa pressure.

2.4.5 Scanning Electron Microscopy (SEM)

SEMs (scanning electron microscopes) are a subset of electron microscopes that use a tightly focused electron beam to produce an image of a sample. A sample's surface interacts with a high-energy electron beam in a succession of ways that reveal details about the sample's morphology and chemical makeup. The various electron-sample interactions are depicted in Figure 2.11(a).

Conductivity is required of the sample for the electron beam to be able to traverse through it. Therefore, in the case of samples that do not conduct electricity, a layer of gold is deposited on the samples outside surface[63].

In a SEM (scanning electron microscope), an electron beam with an energy of 5 to 30 keV is propelled towards the sample and focused by numerous condenser lenses. When this

beam collides with the sample's surface, many collisions between the beam's electrons and the sample's atoms occur. A handful of the sample's outermost electrons will be separated as a result of the collision. Secondary electrons have a lower kinetic energy than primary electrons and can be detected easily by the detector. The number of released electrons is counted by the detector, and the findings are presented on the computer screen. The sample is enlarged by scanning the electron beam over a small region and counting the number of electron beams that emerge from each place. The number of secondary electrons emitted is affected by the sample's topology and atom number.[64]

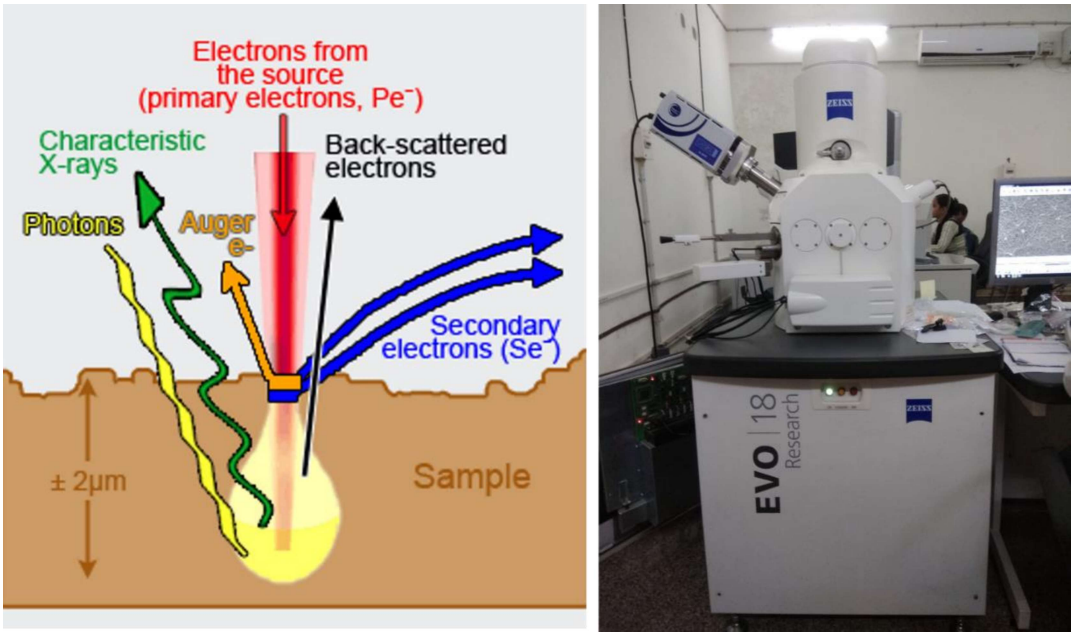

Figure 2.11: (a) Mechanism and **(b)** Experimental setup of SEM measurement (CIF-IIT (BHU)).

Energy dispersive X-ray analysis, a tool used in conjunction with SEM microscopy (EDAX or EDX), is used to investigate the elemental composition. It examines the elemental composition and abundance using X-ray analysis. In this experiment, high-energy electrons

are used to attack the target sample. The incident electrons interact with the electron shell linked to the nucleus, causing it to eject the electrons. An electron jumps from the higher energy shell to the lower energy shell to fill the hole left by the ejection of the electron, releasing energy equal to the difference in the two energy levels [65].

This energy comes out as X-rays, which are called "characteristic X-rays." Each element has its own set of energy levels. Because of this, the X-ray energy produced by each element will be different.

In the present thesis, EVO-MA 15 / 18 scanning electron microscope has been used in which EDS apparatus was attached for the compositional analysis, represented in Fig. 2.11(b).

2.4.6 Ultra – Violet Visible (UV-Vis) Spectroscopy

UV-Vis is a technique that involves absorption and/or reflectance of light (radiation) in the ultraviolet-visible spectral region. UV-Vis absorption spectroscopy measures the attenuation of the light beam after it passes through the sample or after reflection from the surface. The spectrometer measures the light intensity passing through the sample (I) and compares it with the light intensity before passing through the sample (I_o). The ratio of (I/I_0) is defined as transmittance, usually indicated in percentage form (%T). The relation between absorbance (A) and transmittance (T) is defined by the following equation:

$$\mathrm{A} = -\log\left(\frac{\%\mathrm{T}}{100\%}\right) \tag{2.23}$$

The four main components of the spectrometer are (a) light source, (b) sample holder, (c) diffraction grating in a monochromator or prism (d) detector. The radiation source is

usually a Tungsten filament, deuterium arc lamp, Xenon arc lamp, or, more recently, light-emitting diodes. A photomultiplier tube, photodiode, charge couple device (CCD) or a photodiode array is used as a detector. The photomultiplier tube and single photodiode detectors are used with scanning monochromator to filters out all wavelengths and pass only a single wavelength to the detector at one time. The diffraction grating is moved by scanning monochromator by "Step-through" every wavelength so that its intensity can be measured as a function of wavelength.

Using the UV-Vis data, the optical bandgap of the samples under investigation has been established. The absorption data of UV-Vis spectrometer was used to calculate the band gap (E_g) of the material. The band gap is calculated using the Tauc relation. According to the Tauc relation, the optical absorption strength depends on the relationship between the photon energy and band gap:

$$\alpha h\upsilon = A\left(h\upsilon - E_g\right)^n \tag{2.24}$$

where h = Plank's constant, υ = photon's energy, α = absorption coefficient, A = proportionality constant and E_g = band gap. The exponent value n shows the nature of transition, whether allowed or forbidden and direct or indirect.

n = ½ corresponds to direct allowed transition,

n=3/2 corresponds to direct forbidden transition,

n = 2 for indirect allowed transition and

n = 3 for indirect forbidden transition.

The material studied in this thesis has an indirect allowed transition, n = 2.

Figure 2.12: Experimental setup of UV-Visible measurement [JASCO V-770 UV–Vis spectrometer].

2.4.7 Photoluminescence Spectroscopy (PL)

Photoluminescence spectroscopy (PL) is a way to investigate the electrical structure of a material without damaging it. It is a type of luminescence that is started by photoexcitation, which is why the word starts with "photo." In this process, an object takes in photon, which is electromagnetic radiation, and then sends it back out again. In other words, this process describes a jump to a state with more energy, followed by a jump back to a state with less energy and the release of a photon. Between absorption and emission, there is very little time. The selection rules between states are governed by quantum mechanics postulates.

Photoluminescence is a critical technique for determining semiconductor purity and crystalline quality. Extrinsic and intrinsic luminescence are two different types of photoluminescence. A pure material or crystal emits intrinsic luminosity when it emits light. Band to band luminescence, cross luminescence, and exciton luminescence are the three types of intrinsic luminescence that exist. Extrinsic luminescence occurs when impurities or defects are intentionally introduced into a phosphor. Figure 2.13 shows the schematic diagram of a photoluminescence spectrophotometer. This spectrophotometer exhibits a xenon

lamp which is used as an excitation source. This lamp consists of high intensities of all wavelengths. Photoluminescence spectrophotometer is equipped with a monochromator to select a single wavelength used in both processes. The monochromator used in excitation contains two gratings, which decreases stray light, i.e., light with different wavelengths from the chosen one. In addition, to reduce stray light, the monochromator employs concave gratings created through holographic means. Both monochromators are motorized so that wavelength scanning can be done automatically. Photomultiplier tubes are used to detect the fluorescence, which is then multiplied by electronic devices. Typically, the output is presented in a graphical format and saved in a digital format.

Figure 2.13: Mechanism and experimental setup of photoluminescence spectroscopy [Horiba Flourolog 3].

In this thesis, Photoluminescence measurements were done using Photo-luminescence spectrometer Horiba Flourolog 3 (Japan) using Xe (xenon) lamp as an excitation source and slit width of 1nm.

2.4.8 Fourier Transform Infrared Spectroscopy (FTIR)

Infrared (IR) spectroscopy is an important method for the vibrational study of the material. By absorbing infrared light or by a molecule's inelastic light scattering, it can detect molecular vibration. The method is called FTIR spectroscopy because Fourier transform is carried out by the computer to convert raw data to actual spectrum. The spectrum is obtained in a short period of time. It is used to determine the functional group attached to an atom or molecule. A schematic diagram of the Fourier transform infrared spectroscope is shown in Fig. 2.14.

Figure 2.14: (a) Mechanism and **(b)** experimental setup of Fourier transform infrared spectroscopy.

The most important part of the FTIR setup is the interferometer. A Michelson interferometer is usually employed in the FTIR spectrometer. It consists of two mirrors and a beam splitter (semitransparent mirror) placed at an angle of 45° to the fixed and moving mirror. The beam splitter divides the beam and recombines with the fixed and moving mirror so that the recombined beam generates a wavelength-dependent interference pattern.

The incident infrared beam is split in two by the beam splitter, which transmits one half and reflects the other. The two split beams each impact a fixed and movable mirror. The

divided beam then combines once more at the beam splitter to irradiate the sample after reflecting off both mirrors, before being picked up by the detector. The interferogram is cosine Fourier transform of the spectrum, and with the help of data station, the obtained data is Fourier transformed to the recognizable form. Most of the molecular vibration lies in the range of 400-4000 cm^{-1}.

In this thesis work, FTIR spectra of samples were recorded using FT-IR spectrophotometer of Shimadzu, model DF 803 Japan, in transmission mode with the wavenumber range of 400-4000 cm^{-1}. Samples under test were mixed with KBr, pelletized and used for measurement at room temperature.

2.5 Electrical Data Analysis

Electrochemical impedance spectroscopy is a technique for determining a material's electrical properties. Inspection of defects, microstructure, electrical conductivity, and surface chemistry of materials, such as dielectrics and ionic conductors, as well as the adsorbate-adsorbent interface, is beneficial. The conductivity, impedance, dielectric characteristics, and modulus properties of a sample are determined by applying an alternating voltage or current to it.

The electrodes were made on both sides of the pellets using high-temperature platinum paste for the electrical properties evaluation. The platinum-coated pellets were then cured for 30 minutes at 700 ° C. By putting the pellet in the sample holder inside a furnace and using a two-probe LCR setup, the electrical response of several samples was then measured in the ambient atmosphere. The experimental setup used for the characterization is depicted in Figure 2.17. The temperature and frequency-dependent electrical response, such

as dielectric constant, impedance, dielectric loss, complex modulus, etc., were measured with the help of Wayne Kerr 6500P series LCR meter in the temperature range of RT to 700 ºC and frequency range of 24 Hz to1 MHz.

Figure 2.15: Experimental set up of automated impedance analyzer along with sample holder and furnace (6500 P Wayne Kerr, UK)

The phenomenon of ion relaxation and dynamics can be understood with the help of these investigations. Initially, any two parameters can be determined, such as conductance (G) and dissipation factor (D), and the remaining values can be derived using these parameters.

$$\text{Capacitance (C)} = \frac{G}{\omega D} \tag{2.25}$$

$$\text{Conductivity } (\sigma) = G^{*}\left(\frac{d}{A}\right) \tag{2.26}$$

$$\text{Dielectric constant } (\varepsilon_r) = \frac{C*d}{\varepsilon_0*A} \tag{2.27}$$

$$\text{Real part of impedance } (Z') = \frac{D^2}{G*(1+D^2)} \quad (2.28)$$

$$\text{Imaginary part of impedance } (Z'') = \frac{Z'}{D} \quad (2.29)$$

$$\text{Real part of modulus } (M') = \omega * C_0 * Z'' \quad (2.30)$$

$$\text{Imaginary part of modulus } (M'') = \omega * C_0 * Z' \quad (2.31)$$

where A, d, C_0 are the cross-sectional area, thickness of the pellet and capacitance of free space, respectively. The capacitance of free space is given by C = $\frac{A\varepsilon_0}{d}$. After calculating the aforesaid parameters, the detailed study of different spectroscopic analysis has been carried out depending on the characteristics of the materials.

2.5.1 Impedance Spectroscopy Analysis

Polycrystalline materials' dielectric and electrical properties are influenced by (i) bulk or grains, (ii) grain boundaries, and (iii) electrode specimen interface or electrode polarization. It is necessary to separate these contributions in order to comprehend electrical behavior and change its features. Impedance analysis is a useful tool for separating the various components to ceramics' electrical and dielectric properties. Four immittance functions can be used to express the AC response of any material. These are complex impedance (Z*), electric modulus (M*), admittance (Y*), and permittivity (ε*). These are related to each other as:

$$Z^* = Z' - iZ'' = \frac{1}{i\omega C_0 \varepsilon^*} \quad (2.32)$$

$$Y^* = Y^{'} + iY^{"} = \mathrm{i}\omega C_0 \varepsilon^* \quad (2.33)$$

$$M^* = M^{'} + iM^{"} = \frac{1}{\varepsilon^*} \quad (2.34)$$

$$\varepsilon^* = \varepsilon^{'} + i\varepsilon^{"} \quad (2.35)$$

For impedance analysis, two types of plots are generally used. (1) Complex plane plot, like, Z″ vs Z′ and M″ vs M′ plots and (2) Spectroscopic plots like, $\frac{Z^{"}}{Z^{'}}$ or $\frac{M^{"}}{M^{'}}$ vs logʊ plots.

If a polycrystalline sample has all the three contributions, such as grain, grain boundary, and electrode, then each contribution can be presented by an equivalent circuit containing R and C connected in parallel. So, the sample can be represented by an equivalent circuit containing three parallel RC circuits connected in series, as shown in Fig. 2.18. Nyquist plot (Cole-Cole) is majorly applied to calculate the frequency response information of any system by complex impedance function: $Z^*(\omega) = Z'(\omega) - iZ''(\omega)$, where $Z'(\omega)$ and $Z''(\omega)$ are the real and imaginary part of $Z^*(\omega)$. The real and imaginary part of total impedance of equivalent is given by:

$$Z' = \frac{R_g}{(1+\omega R_g C_g)^2} + \frac{R_{gb}}{(1+\omega R_{gb} C_{gb})^2} \quad (2.36)$$

$$Z" = R_g \frac{\omega R_g C_{gb}}{(1+\omega R_g C_g)^2} + R_{gb} \frac{\omega R_{gb} C_{gb}}{(1+\omega R_{gb} C_{gb})^2} \quad (2.37)$$

where, R_g= The bulk(grain) resistance and C_g= capacitance, respectively, and R_{gb} and C_{gb} are the corresponding quantities for interfacial boundary (grain boundary). Frequency can be used to determine where the two arc are in relation to one another on the complex plane.

Because the grain boundary's relaxation period is longer than that of the bulk's, the arc of bulk is in a higher frequency range in the complex plane than is the arc of grain boundary. R_g, R_{gb}, and R_{el} represents the relative contribution from grain, grain boundary, and electrode polarization while C_g, C_{gb}, and C_{el} represents the corresponding capacitive contributions, respectively. In complex plane impedance and modulus analysis, one can observe three semicircular arcs if each of the contributions has a single value of relaxation time, as depicted in Fig. 2.18. Relaxation time (τ), which is equal to the inverse of angular frequency (ω) at which the relaxation peaks occur, is given by the RC product i.e.

$$\tau = 1/\omega = RC \tag{2.38}$$

Real axis intercept equations for various Immittance functions plane plots are given by Hirose and West. The intercepts of the arcs with the real axis (M') give the resistive contributions R_g, R_{gb}, and R_{el} in the impedance plots. The intercepts with M' axis in modulus plots are inversely proportional to the capacitive contributions (C_o/C_g, C_o/C_{gb} and C_o/C_{el}). The value of capacitance from the impedance plot and resistance from the modulus plot can be derived from the peak point frequency in the arc where ωRC = 1 is satisfied. Frequency increase in complex plane impedance and modulus plot are inverse to each other. In the complex impedance plot, electrode polarization appears in the lowest frequency range, followed by grain boundaries in the intermediate frequency range, and gain or bulk contribution appears in the highest frequency range. If the centre of the above three semicircle lies on the real axis, i.e., Z′ and M′, then it means that all the contribution has a single value of relaxation time. Contrary to this, if the centre of the semicircle lies below the real axis, then it means the distribution of relaxation times. The angle α, defined as the angle

which the line joining the origin to the centre of the circle makes with the real axis, is a measure of the distribution of relaxation times of that contribution. The definite numbers of arcs appearing in the complex plane plot also depend on numerous time constants. An electronic specimen having the negligible value of electrode-specimen interface contribution (ohmic contact) can be represented by two parallel RC elements connected in series. Bulk and grain-boundary conductivities σ_g and σ_{gb}, can be calculated respectively using relations $\sigma_g = (1/R_g)\cdot(t/A)$ and $\sigma_{gb} = (R_gC_b / R_{gb}C_{gb}).\sigma_g$ with C being the respective capacitances. The value of capacitance and resistance (i.e., C_g, C_{gb}, R_g, and R_{gb}) can be calculated from the best fit of the Cole-Cole plots at various temperatures. Full, partial, or no semicircle observed in the Cole-Cole plot, depends on the strength of relaxation, experimentally available frequencies and value of distribution parameters. Strenght of relaxation is defined as $\varepsilon_S / \varepsilon_\infty$ where ε_S is the static dielectric constant value as $\omega \rightarrow 0$ and ε_∞ is the dielectric constant as $\omega \rightarrow \infty$ i.e., at optical frequencies. Therefore, it is not astonishing that certain function is favoured on other depending on whether the material being explored is conducting, semiconducting or insulating [Ref]. From the above discussion, impedance plots highlight circuit element (contribution) with large resistance (grain boundaries and electrode-specimen interface) while the modulus plots highlight the contribution with minimum capacitance (bulk contribution). Usually, we see three arc responses related to the bulk, grain boundary, and electrode relaxation. If the frequency range is not the limit, we may see all the processes related to the electrochemical reaction by impedance spectroscopy. However, due to the frequency range limitations of instruments, we can only see some part of the complete response depending upon the temperature. For modelling the impedance spectrum, an equivalent circuit suitable for the system was designed. In actual incidents, the impedance arc

is often depressed, and this leads to the necessity of a constant phase element (CPE). In this case, a constant phase element (CPE) was used instead of a pure capacitor for modelling an equivalent circuit to real impedance data. A constant phase element originates due to the microstructural inhomogeneities inside the sample, and it is equivalent to the distribution of capacitors placed in parallel. The capacitance of the constant phase element is given by the relation C = $Q^K R^{(1-K)/K}$ where the parameter K represents the deviation from ideal capacitive behaviour. The value of K is unity for the pure capacitive behaviour and zero for the pure resistive behaviour. The values of K are calculated from the slope of log |Z| vs log ν plots in the high-frequency regime. At high frequencies, the corrected modulus is monopolized by the imaginary part of the impedance. The modulus approaches zero, according to $|Z|_{adj} \approx f^{-K}$. Thus, the slope on a logarithmic plot has a value of –K at high frequencies. Generally, the K value determines the roughness of the surface. But in the present case, K changes with the temperature, which can be attributed to the formation of ionic charge carriers in comparison to the deformation in the lattice.[66]

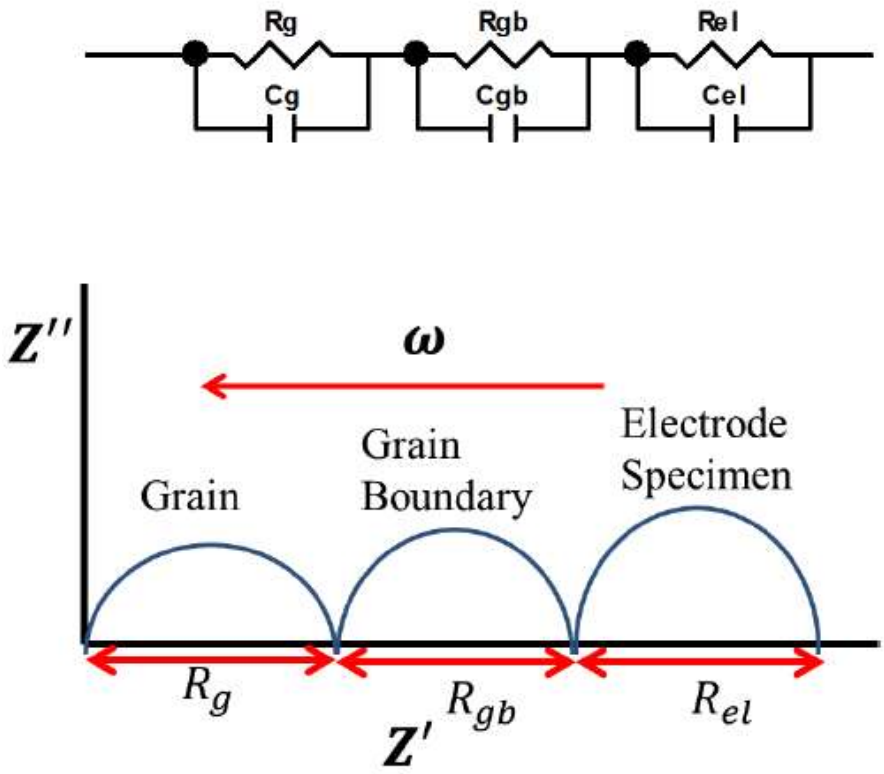

Figure 2.16: The equivalent circuit corresponds to the polycrystalline sample and their frequency response in the complex impedance plot.

2.5.2 Conductivity Spectroscopy Technique

The most effective method for examining electrochemical characteristics is electrical conductivity spectroscopy. Understanding ion dynamics is necessary in order to alter the characteristics of materials that conduct ions. In order to comprehend the ion dynamics in a variety of systems, including glasses, nanocomposite, semiconductors, polymers, polycrystals, etc., different research groups and authors have explored a variety of methodologies. These efforts have been successful in illuminating the conduction process. Both the conduction and the modulus spectra can be used to understand the ion dynamics. In the above description, Jonscher's power (JP) law can be used to determine the real portion of the conductivity of an ionic conductor:

$$\sigma_{ac} = \sigma_o + A\nu^n = \sigma_{dc}\left[1 + \left(\frac{\nu}{\nu_h}\right)^n\right] \quad (2.39)$$

where, σ_o = the frequency-independent conductivity, A = constant, ν = frequency of the applied electric field and ν_h = crossover frequency from dc to the dispersive conductivity region, n = power-law exponent, and it represents the degree of interaction between the mobile ions with the lattice with value generally less than 1.

The above equation has 2 parts: (i) DC conductivity (σ_{dc}), which is independent of frequency and (ii) frequency-dependent ac component. Almond and West suggested crossover frequency as the hopping frequency. The hopping frequency, ν_h and the dc conductivity is associated with each other through the Nernst-Einstein relation:

$$\sigma_{dc} = en_c\mu = \frac{n_c e^2 \gamma \lambda^2}{kT}\upsilon_H \quad (2.40)$$

where n_c = mobile charge carriers concentration, μ = mobility, e = the electronic charge, T = temperature, k = Boltzmann's constant, λ = hopping distance, and γ = the geometrical factor for ion hopping. The charge carrier concentration and its changes with temperature can be assessed using the equation. It is already proved that the conducting spectra of ion-conducting materials at various temperatures follow the scaling law known as the time-temperature superstition principle (TTSP), which means that using the proper scaling settings, onto a single curve, the conductivity isotherm may be superimposed. Mathematically above principle can be written as:

$$\frac{\sigma'(\omega)}{\sigma_{dc}} = F\left(\frac{\upsilon}{\upsilon_s}\right) \quad (2.41)$$

where σ is a temperature-dependent scaling parameter and F is a temperature-independent function. Different researchers have proposed various scaling models, such as Summerfield scaling [67] , Roling et al. scaling, Sidebottom scaling, Baranovskii, and Cordes scaling, and Ghosh scaling. All models differ according to the selection of scaling parameters, i.e., hopping frequency. In Summerfield scaling $\sigma_{dc}T$, in Roling et al., scaling ${\sigma_{dc}T}/{\chi}$ and in Ghosh scaling ω_H are chosen as the scaling parameter. Given that permittivity changes and the Haven ratio are automatically considered, Ghosh scaling is the most extensively used of the aforementioned scaling methods.

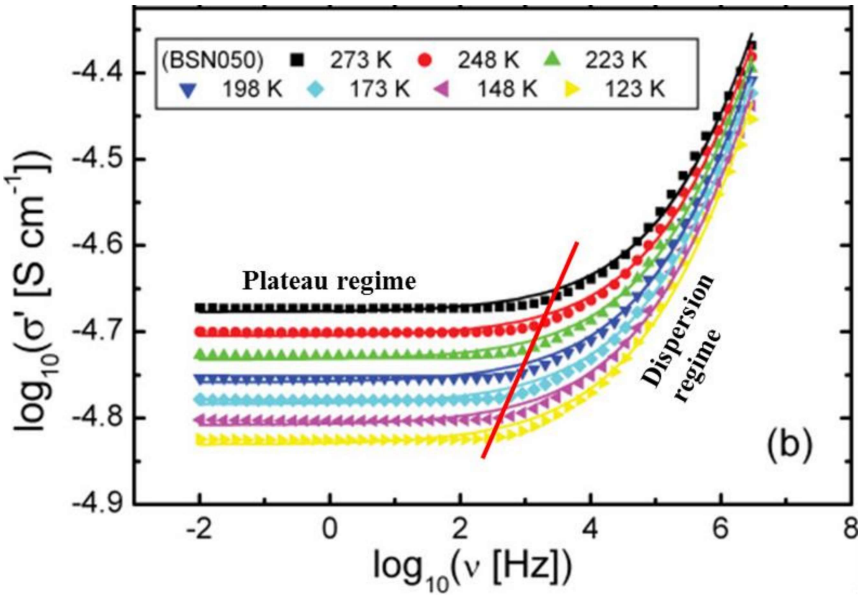

Fig. 2.17: A typical conductivity spectra of a polycrystalline material [67]

2.6 Analysis Techniques

2.6.1 Process of Analysing the Obtained Data

Origin Pro 8.5 program, Soft BV, and the Image-J software were used to examine the structural, optical, and electrical aspects of the tested samples.

2.7 Theoretical Studies

A bond valance site energy (BVSE)-based technique was used to examine the routes taken by the oxide ions during migration. SoftBV was used to calculate the bond valence energy landscape for a test oxide ion. The details are given below.

2.7.1 Bond Valance Energy-Based Approach

An essential method for evaluating the chemical validity of inorganic crystal structures is the Bond Valence model. This model is based on Pauling's electrostatic valence concept's bond-valence sum (BVS) rule, It claims that an atom's total number of bond valences is almost exactly equal to the sum of its oxidation state. With this approach, the sum of bond valences (S_{ij}) about any ion, i, is equal to its valence, V_i (formally known as the oxidation state)

$$V_i = \sum_j S_{ij} \tag{2.42}$$

where the summation runs over all adjacent atoms j of the atom i. valence of the bond A measure of the electrostatic flux between a cation and an anion is known as S_{ij}. It has an inverse relationship with bond length and is directly connected to bond strength. It can be determined by the following relation:

$$S_{ij} = exp\left(\frac{R_o - R_{ij}}{B}\right) \tag{2.43}$$

where R_o and B are constant parameters and R_{ij} = interatomic distance between atoms i and j. The value of B is nearly to 0.37, for many bonds. By calculating the global instability index parameter, the Bond valence technique is also utilized to explain structural aberrations from the ideal 3-dimensional crystal structure. Even though the energy barriers discovered by BVS analysis are just approximate and not as precise as those discovered by more advanced computational techniques. The room-temperature X-ray The parameters from

the Rietveld refined crystallographic information file were utilized to calculate the bond valence energy, and Vesta software was used to construct the BVE landscape and crystal structure. For the calculation, 0.1 was chosen as the spatial resolution. Utilizing the BVE landscape, it was possible to predict the energy barriers for oxide ion.